JOURNAL OF CATALYSIS **176,** 310–320 (1998)
ARTICLE NO. CA982053

Iridium Clusters Supported on γ-Al_2O_3: Structural Characterization and Catalysis of Toluene Hydrogenation

O. Alexeev and B. C. Gates

Department of Chemical Engineering and Materials Science, University of California, Davis, California 95616

Received August 12, 1997; revised February 9, 1998; accepted February 23, 1998

Iridium clusters were prepared on γ-Al_2O_3 that had been calcined at 400°C. When supported $[Ir_4(CO)_{12}]$, the precursor, was treated in H_2 at various temperatures, it was decarbonylated, with aggregation taking place to various degrees to give a family of supported clusters and aggregates with average diameters in the range of about 9 to 33 Å, as determined by extended X-ray absorption fine structure (EXAFS) spectroscopy. Similarly, samples were decarbonylated in He, and the degree of aggregation of the iridium was less than in H_2 under comparable conditions. Infrared spectra show that decarbonylation of the supported $[Ir_4(CO)_{12}]$ in the presence of H_2 was not reversible and was accompanied by aggregation of the iridium; infrared spectra of CO adsorbed on the decarbonylated samples were characterized by a band at 2058 cm^{-1}, typical of terminal CO adsorbed on iridium particles. The γ-Al_2O_3-supported iridium clusters and aggregates were used to catalyze toluene hydrogenation at 60°C and 1 atm. Samples with nearly the same Ir–Ir first-shell coordination number (nearly the same dispersion) were characterized by essentially the same catalytic activity, independent of whether the decarbonylation was carried out in He or H_2. The catalytic activity for the structure-insensitive toluene hydrogenation reaction was found to increase with increasing average cluster or aggregate diameter and to be greater for iridium on the calcined γ-Al_2O_3 than for iridium on uncalcined γ-Al_2O_3. © 1998 Academic Press

INTRODUCTION

Supported catalysts consisting of metal clusters smaller than about 10–20 Å in diameter are difficult to characterize because of the smallness and nonuniformity of the clusters, and there is little information available providing relationships between cluster size and catalytic activity. Clusters as small as these are important in practical catalysts, e.g., platinum clusters consisting of about 5–10 atoms each, on average, in zeolite LTL (1–5) applied for selective dehydrocyclization of naphtha to give aromatics (6–7). Supported clusters that appear to have relatively high degrees of structural uniformity have been made by decarbonylation of supported metal carbonyl cluster precursors such as $[Ir_4(CO)_{12}]$ (8).

Continuing an investigation of supported clusters made from $[Ir_4(CO)_{12}]$, we report the preparation of a family of γ-Al_2O_3-supported iridium catalysts, their characterization by extended X-ray absorption fine-structure (EXAFS) spectroscopy, and their catalytic activities for toluene hydrogenation. The samples were prepared with γ-Al_2O_3 that had been calcined at 400°C; the results complement those reported (9) for similar samples prepared with uncalcined γ-Al_2O_3. The data demonstrate a dependence of catalytic activity on cluster size, even for the structure-insensitive toluene hydrogenation, and an effect of the calcination temperature of the γ-Al_2O_3.

EXPERIMENTAL METHODS

Materials

$[Ir_4(CO)_{12}]$ (Strem) was used as supplied. *n*-Pentane solvent (Aldrich) was refluxed under N_2 in the presence of Na/benzophenone ketyl (to remove traces of water) and deoxygenated by sparging of dry N_2. All gases were UHP grade and additionally purified by flow through traps containing pellets of Al_2O_3-supported Cu and activated zeolite to remove traces of O_2 and H_2O, respectively. The γ-Al_2O_3 support was prepared by first forming a paste of porous γ-Al_2O_3 (Degussa, Aluminum Oxide C) and deionized water, followed by overnight drying at 120°C, calcination at 400°C in flowing O_2 (Matheson) for 2 h, and evacuation (10^{-3} Torr) at 400°C for 14 h. The surface area of the resultant material was approximately 100 m^2/g.

Preparation and Decarbonylation of γ-Al_2O_3-Supported $[Ir_4(CO)_{12}]$

The preparation procedures are as described elsewhere (10). $[Ir_4(CO)_{12}]/\gamma$-Al_2O_3 was decarbonylated by treatment in flowing H_2 as the temperature was ramped at a rate of 3°C/min from 25°C to the desired temperature and then held at that temperature for 2 h. The sample containing supported iridium clusters that had aggregated was formed by treatment of $[Ir_4(CO)_{12}]/\gamma$-Al_2O_3 in H_2 at 400°C for 2 h, followed by treatment with O_2 at 300°C for 1 h and then reduction in H_2 at 400°C for 2 h.

0021-9517/98 $25.00

Infrared Spectroscopy

The γ-Al_2O_3-supported iridium carbonyls, their decarbonylation, and subsequent recarbonylation were characterized by infrared spectroscopy, as described elsewhere (10).

Catalytic Hydrogenation of Toluene

Toluene hydrogenation was carried out in a once-through tubular flow reactor at 60°C and atmospheric pressure. Prior to reaction, each catalyst sample was treated in H_2 as the temperature was ramped at a rate of 3°C/min to the desired value (in the range of 100–400°C) and held for 2 h. An Isco 260D pump was used to feed liquid toluene to a tube packed with particles of inert α-Al_2O_3, where it vaporized and was mixed with flowing H_2. The toluene and H_2 partial pressures at the reactor inlet were 50 and 710 Torr, respectively. The products flowed from the reactor to an on-line gas chromatograph for analysis; the instrument was equipped with a flame ionization detector. Conversions of toluene were less than 1%. There was no measurable conversion of toluene in the absence of catalyst. Accuracy in the determination of reaction rates (from differential conversions) was ±10%. Calculations with standard methods showed that the influence of transport phenomena on the reaction rate was negligible.

EXAFS Spectroscopy

EXAFS experiments were performed at X-ray beamline 2–3 of the Stanford Synchrotron Radiation Laboratory (SSRL) at the Stanford Linear Accelerator Center, Stanford, California, and at beamline X-11A at the National Synchrotron Light Source (NSLS), Brookhaven National Laboratory, Upton, NY. The storage ring at SSRL operated with an electron energy of 3 GeV; the ring current was 60–100 mA. The ring energy at NSLS was 2.5 GeV; the ring current was at least 110 mA.

EXAFS spectroscopy was used to characterize variously decarbonylated iridium clusters formed from supported $[Ir_4(CO)_{12}]$; the samples, initially containing $[Ir_4(CO)_{12}]$, were treated in H_2 under conditions to give various degrees of decarbonylation (and various degrees of aggregation of the iridium). Similarly, samples were prepared by treatment in He instead of H_2, as reported previously (10). Each powder sample was pressed into a wafer with a C-clamp in a glovebox at the synchrotron. The sample mass was calculated to give an absorbance of about 2.5 at the Ir L_{III} absorption edge to optimize the signal to noise ratio. After each sample had been pressed, it was loaded into an EXAFS cell (11), sealed under a positive N_2 pressure, and removed from the drybox. The sample was then treated in flowing purified H_2 while being heated to 100–400°C at a rate of 3°C/min and then held at the desired temperature for 2 h; it was then cooled to room temperature in flowing H_2, evacuated to 10^{-5} Torr, and aligned in the X-ray beam.

The EXAFS data were recorded in the transmission mode after the cells had been cooled to nearly liquid nitrogen temperature. The data were collected with a double crystal monochromator [Si(220) at SSRL or Si(111) at NSLS] which was detuned 15% to minimize the effects of higher harmonics in the X-ray beam. The samples were scanned at energies near the Ir L_{III} absorption edge (11215 eV).

EXAFS Reference Data

The EXAFS data were analyzed with experimentally determined reference files obtained from EXAFS data characterizing materials of known structure, as stated elsewhere (10).

EXAFS DATA ANALYSIS

The EXAFS data were extracted from the spectra with the XDAP software (12). The EXAFS function characterizing each sample was obtained from the X-ray absorption spectrum by a cubic spline background subtraction and normalized by dividing the absorption intensity by the height of the absorption edge. The normalized EXAFS function representing each sample was obtained from the average of six scans. The main contributions to the spectra were isolated by inverse Fourier transformation of the normalized EXAFS function. The analysis was done with the Fourier-filtered data.

The parameters characterizing interactions of Ir with both low-Z (O, C) and high-Z (Ir) scatterers were determined by multiple-shell fitting in r space (where r is the distance from the absorbing atom, Ir) and in k space (k is the wave vector) with application of k^1 and k^3 weighting in the Fourier transformation. The fit was optimized by use of the difference file technique (13, 14) with phase- and amplitude-corrected Fourier transforms.

The data characterizing the samples treated with H_2 at different temperatures were analyzed as follows: The raw data at the Ir L_{III} edge characterizing the sample initially consisting of $[Ir_4(CO)_{12}]/\gamma$-Al_2O_3 following treatment in H_2 at 100°C were Fourier transformed with k^3 weighting over the range $2.83 < k < 15.84$ Å^{-1}, with no phase correction. The Fourier-transformed data were then inverse transformed in the range $0.31 < r < 4.41$ Å. The analysis was done with 20 free parameters over the range $3.61 < k < 15.0$ Å^{-1} and $0.31 < r < 4.00$ Å. The statistically justified number of free parameters, n, was found to be 27, as estimated from the Nyquist theorem (15), $n = (2\Delta k \Delta r/\pi) + 1$, where Δk and Δr, respectively, are the k and r ranges used to fit the data. With the difference file technique (13, 14), the Ir–Ir contribution, the largest in the EXAFS spectrum, was estimated first and subtracted from the raw data. The residual

spectrum was expected to represent Ir–$O_{support}$ and Ir–CO* contributions (O* is carbonyl oxygen). The Ir–$O_{support}$ contributions were expected at both relatively short and long distances (16), corresponding to the contributions designated (Ir–O_s) and (Ir–O_l), respectively. After optimization of the parameters representing the Ir–$O_{support}$, Ir–C, and Ir–O* contributions, the first-guess Ir–Ir contributions were added and the resulting spectrum compared with the raw data. Parameters giving the best fit for the Ir-high-Z (Ir–Ir) and Ir-low-Z (Ir–$O_{support}$ and Ir–CO*) contributions were determined by multiple-shell fitting in r space and in k space with phase- and amplitude-corrected Fourier transforms (15, 17).

A similar procedure was applied to the raw EXAFS data at the Ir L_{III} edge obtained for the sample initially consisting of $[Ir_4(CO)_{12}]/\gamma$-Al_2O_3 after treatment with H_2 at temperatures in the range of 200–400°C. The raw EXAFS data were Fourier transformed with k^3 weighting over the range $3.68 < k < 15.95$ Å^{-1}, with no phase correction. The Fourier-transformed data were then inverse transformed in the range $0.20 < r < 4.0$ Å. The analysis was done with 20 free parameters over the range $4.0 < k < 15.0$ Å^{-1} and $0.20 < r < 4.0$ Å. The statistically justified number of free parameters, estimated as described above, was about 27.

After subtraction of first-guess Ir–Ir and Ir–$O_{support}$ contributions from the raw data characterizing the sample that had been treated with H_2 at 200°C, the residual spectrum showed no evidence of Ir–CO* contributions. Hence, optimization of the parameters was done by multiple shell fitting taking into account only Ir–Ir and Ir–$O_{support}$ contributions. However, the fit was not satisfactory in the low-Z (low-k) region, and another contribution was included; this was postulated to be an Ir–Al contribution. A satisfactory fit was obtained when Ir–Ir, Ir–$O_{support}$, and Ir–Al contributions were included. We emphasize that the postulated Ir–Al contribution was always small.

In addition to these contributions, second-shell Ir–Ir contributions were accounted for in the analysis of data characterizing samples that had been treated in H_2 at temperatures higher than 200°C.

RESULTS

Preparation of Supported Iridium Clusters by Treatment of γ-Al_2O_3-Supported $[Ir_4(CO)_{12}]$ in H_2

As γ-Al_2O_3-supported $[Ir_4(CO)_{12}]$ was treated in flowing H_2 with the temperature being ramped from 25 to 300°C, decarbonylation occurred, as shown by infrared spectra in the υ_{CO} region (Fig. 1). The υ_{CO} bands assigned to supported $[Ir_4(CO)_{12}]$ [2112, 2072, 2029, and 2002 cm^{-1} (18)] declined in intensity as the temperature increased, disappearing at about 300°C and indicating virtually complete decarbonylation.

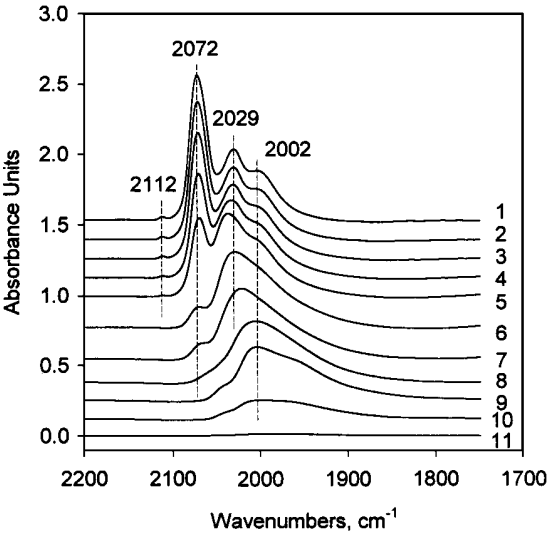

FIG. 1. Infrared spectra in the υ_{CO} region characterizing decarbonylation of γ-Al_2O_3-supported $[Ir_4(CO)_{12}]$ in H_2 flow under the following conditions: 1, 50°C; 2, 70°C; 3, 80°C; 4, 90°C; 5, 100°C; 6, 2 h at 100°C; 7, 150°C; 8, 2 h at 150°C; 9, 2 h at 200°C; 10, 2 h at 250°C; 11, 300°C.

Recarbonylation and Decarbonylation of γ-Al_2O_3-Supported Iridium Clusters

After γ-Al_2O_3-supported $[Ir_4(CO)_{12}]$ had been decarbonylated by treatment in H_2 at 300°C, the sample was exposed to CO at different temperatures in attempts to recarbonylate the clusters. When the decarbonylated sample was treated with CO at room temperature, the resultant spectrum (Fig. 2, spectrum 1) was different from that of γ-Al_2O_3-supported $[Ir_4(CO)_{12}]$ (Fig. 1, spectrum 1) and characterized by a broad, intense band at 2058 cm^{-1} (Fig. 2,

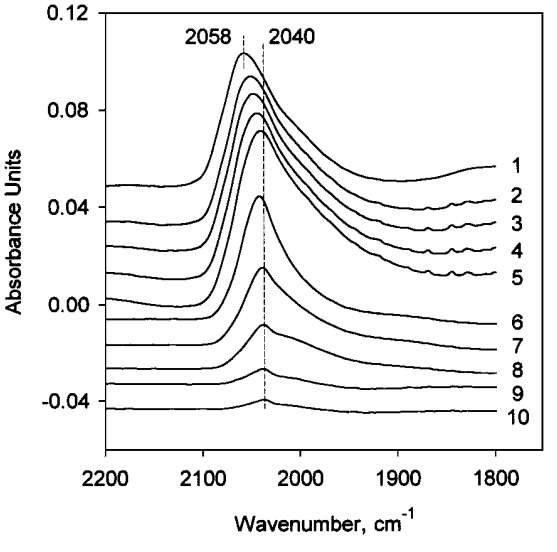

FIG. 2. Infrared spectra of CO adsorbed on sample prepared from $[Ir_4(CO)_{12}]$ on γ-Al_2O_3 and treated with H_2 at 300°C, following treatment in He under the following conditions: 1, 25°C; 2, 70°C; 3, 90°C; 4, 110°C; 5, 130°C; 6, 160°C; 7, 180°C; 8, 200°C; 9, 240°C; 10, 260°C.

spectrum 1), which is assigned to terminal CO on supported iridium particles (19). This result indicates that the decarbonylation of γ-Al_2O_3-supported $[Ir_4(CO)_{12}]$ in the presence of H_2 was not reversible under these conditions and suggests that structural changes of the cluster framework took place.

In subsequent experiments, the adsorbed CO was removed from the sample by flowing He as the temperature was ramped from 25 to 300°C at a rate of 3°C/min; the band at 2058 cm^{-1} shifted to 2040 cm^{-1}, declined in intensity, and, when the temperature reached 260°C, disappeared (Fig. 2). When this decarbonylated sample was exposed to CO again at room temperature, the band at 2058 cm^{-1} reappeared, indicating that this second-stage decarbonylation was reversible. Moreover, when the re-decarbonylated sample was exposed to CO at 200°C for 8 h, the infrared spectrum became virtually identical to that recorded after treatment of the originally decarbonylated sample with CO at room temperature (Fig. 2, spectrum 1).

In summary, the infrared spectra indicate that decarbonylation of $[Ir_4(CO)_{12}]$ supported on γ-Al_2O_3 in the presence of H_2 is not reversible. The similarity between the spectra characterizing the samples after decarbonylation and subsequent exposure to CO and the spectra of CO adsorbed on iridium metal suggests that the clusters aggregated during the initial decarbonylation in the presence of H_2.

EXAFS Data Characterizing Supported Iridium Clusters and Aggregates

The results of the data fitting for the samples treated with H_2 at various temperatures are summarized in Tables 1 and 2. Comparisons of representative raw data and fits, in k space and r space, are shown in Fig. 3. The residual spectra determined by subtracting the Ir–Ir + Ir–$O_{support}$ contributions from the raw EXAFS data (which give evidence of the Ir–C and Ir–O* contributions) are shown in Figs. 3D and 3E, respectively. The best-fit EXAFS parameters are summarized in Tables 1 and 2. The XDAP software (12) was used to obtain rough estimates of the error bounds in these parameters (Tables 1 and 2). These error bounds represent precisions determined from statistical analysis of the data, not accuracies.

The increases in the Ir–Ir contributions (Table 1) with increasing temperature of treatment in H_2 show that the

TABLE 1

EXAFS Results at the Ir L_{III} Edge Characterizing the Species Formed by Decarbonylation of $[Ir_4(CO)_{12}]$ on γ-Al_2O_3 in H_2 at Different Temperatures[a]

Treatment temperature in H_2, °C	Shell	N	R (Å)	$10^3 \cdot \Delta\sigma^2$ (Å^2)	ΔE_0 (eV)	EXAFS reference
100	Ir–Ir	2.9 ± 0.1	2.67 ± 0.01	7.2 ± 0.4	7.6 ± 0.5	Pt–Pt
	Ir–$O_{support}$					
	Ir–O_s	0.7 ± 0.1	2.15 ± 0.01	10.0 ± 0.9	−14.1 ± 0.9	Pt–O
	Ir–O_l	1.4 ± 0.1	2.79 ± 0.01	−5.1 ± 0.1	−10.2 ± 0.4	Pt–O
	Ir–CO					
	Ir–C	1.5 ± 0.1	1.87 ± 0.01	1.8 ± 0.2	−7.6 ± 0.6	Ir–C
	Ir–O*	1.2 ± 0.1	2.99 ± 0.01	1.6 ± 0.2	7.0 ± 0.3	Ir–O*
200	Ir–Ir	5.1 ± 0.1	2.68 ± 0.01	2.2 ± 0.1	−0.6 ± 0.3	Pt–Pt
	Ir–$O_{support}$					
	Ir–O_s	0.9 ± 0.1	2.16 ± 0.01	8.8 ± 1.2	−4.5 ± 0.7	Pt–O
	Ir–O_l	1.1 ± 0.1	2.68 ± 0.01	0.0 ± 0.3	−12.8 ± 0.5	Pt–O
	Ir–Al[b]	0.4 ± 0.1	1.79 ± 0.01	5.1 ± 0.7	−6.3 ± 1.0	Ir–Al
300	Ir–Ir (first-shell)	6.5 ± 0.1	2.68 ± 0.01	3.2 ± 0.1	−0.6 ± 0.1	Pt–Pt
	Ir–Ir (second-shell)	1.0 ± 0.1	3.83 ± 0.01	2.7 ± 0.4	−4.0 ± 0.5	Pt–Pt
	Ir–$O_{support}$					
	Ir–O_s	0.7 ± 0.1	2.14 ± 0.01	7.9 ± 0.9	−2.1 ± 0.6	Pt–O
	Ir–O_l	0.7 ± 0.1	2.76 ± 0.01	−2.1 ± 1.1	−15.3 ± 0.2	Pt–O
	Ir–Al[b]	0.4 ± 0.1	1.78 ± 0.01	7.2 ± 0.7	−6.3 ± 1.0	Ir–A1
400	Ir–Ir (first-shell)	7.1 ± 0.2	2.68 ± 0.01	4.3 ± 0.3	−1.3 ± 0.3	Pt–Pt
	Ir–Ir (second-shell)	1.0 ± 0.2	3.80 ± 0.02	2.5 ± 0.8	−6.3 ± 1.0	Pt–Pt
	Ir–$O_{support}$					
	Ir–O_s	0.6 ± 0.1	2.17 ± 0.01	5.2 ± 1.9	−2.8 ± 1.3	Pt–O
	Ir–O_l	0.6 ± 0.1	2.76 ± 0.01	−0.7 ± 0.9	−15.7 ± 0.7	Pt–O
	Ir–Al[b]	0.4 ± 0.1	1.82 ± 0.01	6.3 ± 1.3	−17.9 ± 1.0	Ir–Al

[a] Notation: N, coordination number; R, distance between absorber and backscatterer atom; $\Delta\sigma^2$, Debye–Waller factor; ΔE_0, inner potential correction; the subscripts s and l refer to short and long, respectively.

[b] Assignment of backscatterer tentative.

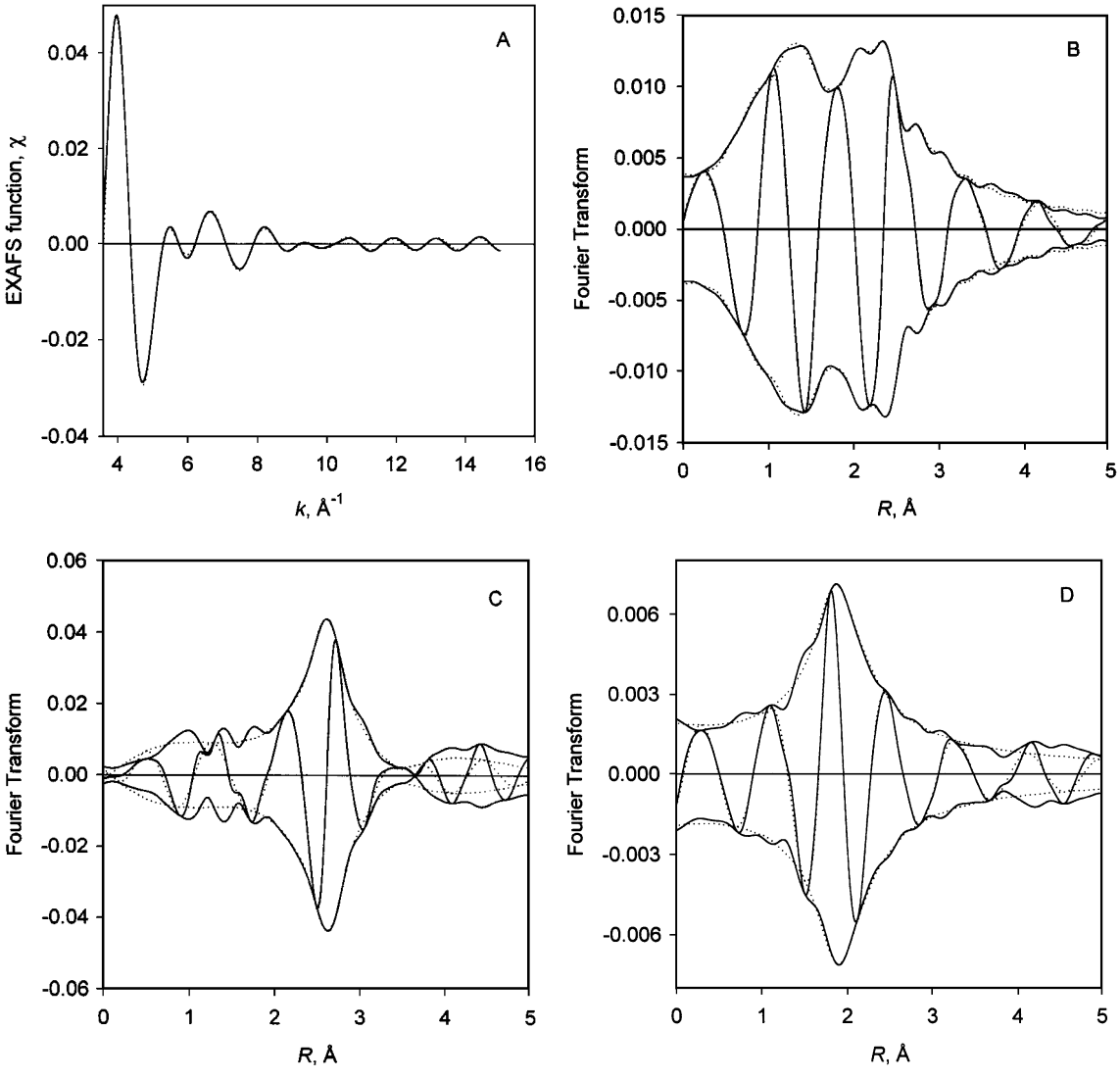

FIG. 3. Results of EXAFS analysis at the Ir L_{III} edge obtained with the best calculated coordination parameters characterizing supported iridium clusters formed by the decarbonylation of γ-Al_2O_3-supported $[Ir_4(CO)_{12}]$ in flowing H_2 at 100°C: A, experimental EXAFS function (solid line) and sum of the calculated Ir–Ir + $Ir–O_{support}$ (Ir–O_s and Ir–O_l) + Ir–CO (Ir–C and Ir–O*) contributions (dotted line); B, imaginary part and magnitude of uncorrected Fourier transform (k^0 weighted, $\Delta k = 3.61$–15.00 Å^{-1}) of experimental EXAFS (solid line) and sum of the calculated Ir–Ir + $Ir–O_{support}$ (Ir–O_s and Ir–O_l) + Ir–CO (Ir–C and Ir–O*) contributions (dotted line); C, imaginary part and magnitude of phase- and amplitude-corrected Fourier transform (k^0 weighted, $\Delta k = 3.61$–15.00 Å^{-1}) of raw data minus the calculated Ir–$O_{support}$ (Ir–O_s and Ir–O_l) + Ir–CO (Ir–C and Ir–O*) contributions (solid line) and calculated Ir–Ir contributions (dotted line); D, residual spectrum illustrating Ir–C contributions of carbonyl ligands: imaginary part and magnitude of phase-corrected Fourier transform (k^0 weighted, $\Delta k = 3.61$–15.00 Å^{-1}) of raw data minus the calculated Ir–Ir + Ir–$O_{support}$ + Ir–O* contributions (solid line) and calculated Ir–C contributions (dotted line); (E) residual spectrum illustrating Ir–O* contributions of carbonyl ligands: imaginary part and magnitude of phase-corrected Fourier transform (k^0 weighted, $\Delta k = 3.61$–15.00 Å^{-1}) of raw data minus the calculated Ir–Ir + Ir–$O_{support}$ + Ir–C contributions (solid line) and calculated Ir–O* contributions (dotted line); (F) residual spectrum illustrating the contributions of metal–support interactions: imaginary part and magnitude of phase-corrected Fourier transform (k^0 weighted, $\Delta k = 3.61$–15.00 Å^{-1}) of raw data minus the calculated Ir–Ir + Ir–CO (Ir–C and Ir–O*) contributions (solid line) and calculated Ir–$O_{support}$ (Ir–O_s + Ir–O_l) contributions (dotted line).

iridium aggregated during these treatments, consistent with the infrared results. We now refer to decarbonylated species with nuclearities (numbers of Ir atoms), essentially the same as those of the precursor $[Ir_4(CO)_{12}]$, as clusters and to the larger species as aggregates.

Toluene Hydrogenation Catalyzed by Supported Iridium Clusters and Aggregates

The toluene hydrogenation data characterizing supported catalysts that had been decarbonylated under

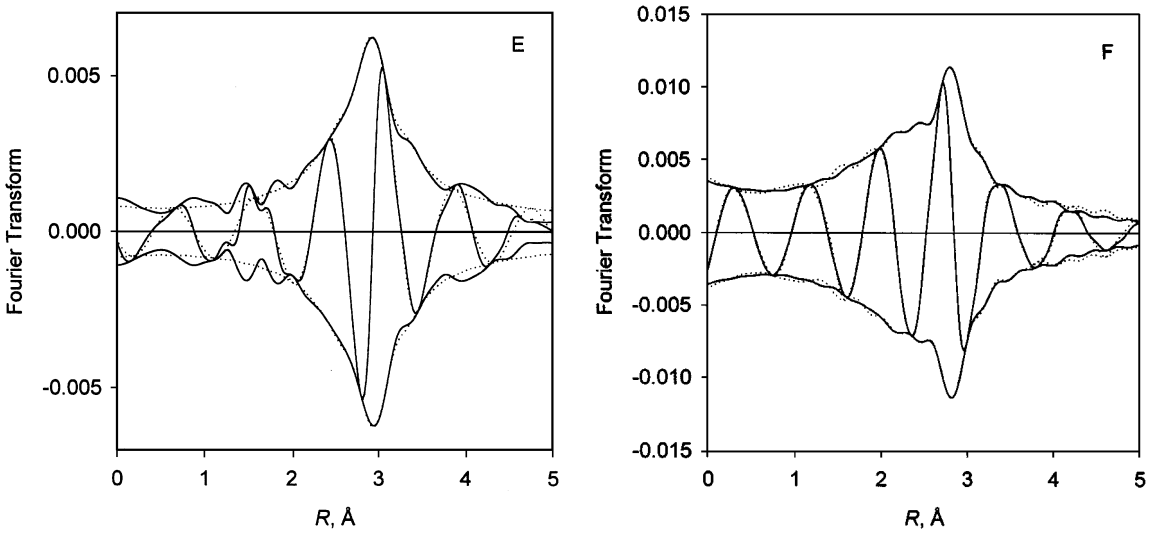

FIG. 3—*Continued*

various conditions are summarized in Table 3. Table 3 includes data characterizing the samples treated in H_2 and those treated in He (the infrared and EXAFS data characterizing the latter samples are presented elsewhere (10)). The catalytic activities represented here as turnover frequencies were determined from data recorded when each catalyst sample had been on stream in the flow reactor for 2 h, which corresponds to virtual steady-state operation. Turnover frequencies were calculated from reaction rates (determined from differential conversions) by taking into account iridium dispersions estimated from the Ir–Ir first-shell coordination numbers on the basis of the assumption that the clusters or aggregates were spherical (details are given below). The apparent activation energies calculated from the temperature dependencies of the reaction rates were found to be 10–13 kcal/mol, about the same as the values observed for other supported iridium catalysts for this reaction (20).

The data of Table 3 show a pattern of catalytic activity as a function of iridium dispersion. Some of these data are compared in Table 4 with data already reported for the toluene hydrogenation catalyzed by γ-Al_2O_3-supported iridium clusters. Comparison of the new and reported data illustrates how the support pretreatment conditions and iridium dispersion (cluster or aggregate size) influence the catalytic activity.

DISCUSSION

Preparation of Supported Iridium Clusters by Treatment of Supported $[Ir_4(CO)_{12}]$ in H_2

The υ_{CO} infrared data (Fig. 1) show that γ-Al_2O_3-supported $[Ir_4(CO)_{12}]$ was stable in H_2 only at temperatures $<50^\circ$C; upon heating in H_2 at 50–100°C, substantial decarbonylation was observed (Fig. 1). The EXAFS data (Table 1) provide evidence of the structures of the supported clusters formed as a result of treatment in H_2 at 100°C. The first-shell Ir–Ir coordination number was found to be 2.9, which is indistinguishable within

TABLE 2

Ir L_{III} Edge EXAFS Results Characterizing the Species Formed by Decarbonylation of $[Ir_4(CO)_{12}]$ on γ-Al_2O_3 in H_2 at 400°C Followed by Treatment in O_2 at 300°C and then H_2 at 400°C[a]

Shell	N	R (Å)	$10^3 \cdot \Delta\sigma^2$ (Å^2)	ΔE_0 (eV)	EXAFS reference
Ir–Ir (first-shell)	10.0 ± 0.1	2.69 ± 0.01	2.4 ± 0.1	-1.1 ± 0.1	Pt–Pt
Ir–Ir (second-shell)	3.0 ± 0.1	3.83 ± 0.01	1.7 ± 0.1	-5.0 ± 0.2	Pt–Pt
$Ir–O_{support}$					
$Ir–O_s$	0.3 ± 0.1	2.08 ± 0.01	-2.9 ± 0.4	2.0 ± 1.0	Pt–O
$Ir–O_l$	0.6 ± 0.1	2.81 ± 0.01	-9.8 ± 0.1	-13.6 ± 0.2	Pt–O
Ir–Al[b]	0.3 ± 0.1	1.77 ± 0.01	-0.1 ± 0.3	15.4 ± 0.9	Ir–Al

[a] Notation as in Table 1.
[b] Assignment of backscatterer tentative.

TABLE 3

Dispersions of Supported Iridium Catalysts and Catalytic Activities for Toluene Hydrogenation[a]

Treatment gas	Temperature, °C	N_{Ir-Ir}[b]	D, Å[c]	Ir_s/Ir_t[d]	Activity, $10^3 \cdot$ TOF, s^{-1}	Reference
He	300	3.0	5.3	1.00	10.9	This work[e]
He	400	5.2	9.4	0.97	14.9	This work[e]
H_2	200	5.1	9.3	0.98	17.2	This work
H_2	300	6.5	11.3	0.84	39.8	This work
H_2	400	7.1	12.5	0.78	55.3	This work
O_2 then H_2	300 then 400	10.0	32.6	0.39	140.8	This work

[a] Reaction at 60°C, $P_{toluene} = 50$ Torr and $P_{H_2} = 710$ Torr.
[b] First-shell Ir–Ir coordination number estimated on the basis of EXAFS data.
[c] Diameter of metal clusters determined from EXAFS data on basis of calculations reported by Kip *et al.* (22).
[d] Calculated dispersion (22) expressed as the ratio of the number of surface iridium atoms to total number of iridium atoms in the clusters or aggregates.
[e] EXAFS characterization reported elsewhere (10).

experimental error from that observed for the γ-Al_2O_3-supported $[Ir_4(CO)_{12}]$ precursor (10). The implication is that the iridium cluster nuclearity did not change after heating of $[Ir_4(CO)_{12}]/\gamma$-Al_2O_3 in H_2 at 50–100°C. Thus, the clusters formed under these conditions are approximated as tetrairidium. A comparison of the Ir–C and Ir–O* contributions in the EXAFS spectrum (Table 1) with those characterizing supported $[Ir_4(CO)_{12}]$ (10) indicates that only about 50% of the CO ligands had been removed from the clusters after this treatment. The partial removal of the CO ligands was accompanied by increased Ir-support interactions, as indicated by the Ir–O contribution at a bonding distance of 2.15 Å (Table 1) (which is somewhat shorter than that observed for untreated γ-Al_2O_3-supported $[Ir_4(CO)_{12}]$ at 2.29 Å (10)) and the longer $Ir-O_l$ contribution at 2.79 Å (Table 1). In addition to these Ir–O contributions, others, suggested to be Ir–Al, were observed as the decarbonylation proceeded (Table 1). These latter contributions are small and not determined with a high degree of confidence, and they are only tentatively attributed to interactions between Ir atoms and Al^{3+} ions of the support. Such Ir–Al interactions have been suggested previously for iridium clusters prepared by decarbonylation of $[Ir_6(CO)_{15}]^{2-}$ (20) and of $[Ir_4(CO)_{12}]$ (21) on γ-Al_2O_3.

TABLE 4

Toluene Hydrogenation Catalyzed by γ-Al_2O_3-Supported Iridium Clusters at 60°C (the Supported Precursor was $[Ir_4(CO)_{12}]$ in Each Sample)

Support treatment	Decarbonylation conditions	N_{Ir-Ir}[a]	Activity, $10^3 \cdot$ TOF, (s^{-1})	Reference
No calcination; evacuation at 25°C	He, 300°C	2.9	0.9	(9)
Calcination in air at 100°C followed by evacuation at 25°C	He, 300°C	3.0	1.6	(21)
Calcination in air at 400°C followed by evacuation at 400°C	He, 300°C	3.0	10.9	This work[b]
No calcination; evacuation at 25°C	He at 300°C followed by H_2 at 300°C	7.7	26.0	(9)
Calcination in air at 100°C followed by evacuation at 25°C	He at 400°C followed by H_2 at 400°C	7.2	13.9	(21)
Calcination in air at 400°C followed by evacuation at 400°C	H_2, 300°C	7.1	55.3	This work

[a] Ir–Ir first-shell coordination number.
[b] EXAFS characterization reported elsewhere (10).

As the interactions of the Ir atoms with the support affect the interaction of the Ir atoms with CO ligands, we suggest that the increase in the Ir-support interactions resulting from partial decarbonylation may explain (at least in part) the broadening of the υ_{CO} bands at 2029 and 2002 cm^{-1} in the infrared spectra (Fig. 1). Accompanying the broadening of these bands as the temperature of H_2 treatment increased from 50 to 100°C, the υ_{CO} bands at 2112 and 2072 cm^{-1} (assigned to supported $[Ir_4(CO)_{12}]$ (18)) disappeared first. We suggest, on the basis of these results, that the first stages of decarbonylation of $[Ir_4(CO)_{12}]$ took place with the tetrahedral metal frame of the cluster essentially intact.

The infrared data (Fig. 1) show that treatment of the sample with H_2 at 200°C led to further removal of CO ligands, with complete decarbonylation being observed at 300°C. (The EXAFS data characterizing the sample treated with H_2 at 200°C (Table 1), in contrast to the infrared data, no longer give evidence of remaining CO ligands; the difference between the results of the two characterization methods is consistent with the lower sensitivity of EXAFS spectroscopy).

The EXAFS data clearly demonstrate that treatment of γ-Al_2O_3-supported $[Ir_4(CO)_{12}]$ in H_2 at temperatures of 200°C and higher led to some aggregation of the iridium. For example, the first-shell Ir–Ir coordination number was found to be 5.1 after the treatment at 200°C, and the value increased with increasing temperature of treatment (Table 1). As the Ir–Ir first-shell contributions increased, the Ir-support contributions ($Ir-O_s$ and $Ir-O_l$) decreased (Table 1). These results are consistent with the conclusion that a decreasing fraction of Ir atoms resided at the metal-support interface as the aggregate nuclearity increased.

Thus, the infrared and EXAFS data show that the treatments in H_2 led to decarbonylation of the supported $[Ir_4(CO)_{12}]$ accompanied by aggregation of the iridium, leading to a family of samples consisting of supported iridium clusters and aggregates with various average sizes. These data, combined with those characterizing the samples prepared by treating the supported $[Ir_4(CO)_{12}]$ in He (10), show a difference between decarbonylation in He and that in H_2. The removal of CO ligands took place at lower temperatures in the presence of H_2 than in the presence of He. At a given temperature, the degree of aggregation of the iridium in the presence of H_2 exceeded the degree of aggregation in the presence of He (Table 3).

In summary, the decarbonylation of γ-Al_2O_3-supported $[Ir_4(CO)_{12}]$ in H_2 led to faster removal of CO ligands from the clusters than decarbonylation in He, and it was accompanied by greater aggregation of the iridium than occurred in the presence of He at the same temperature.

Dispersion of Supported Iridium Clusters and Aggregates

The EXAFS data allow estimates of the iridium cluster and aggregate sizes and dispersions. The estimates are based on the model of Kip *et al.* (22), who calculated the shapes of the metal clusters or particles as a function of the relative magnitude of the metal–metal and metal–support interaction energy by minimizing the total energy, assuming the fcc metal structure, and an epitaxial location of the metal atoms on the (111) surface of the support. The results (Table 3) show a wide range of cluster and aggregate sizes, depending on the temperature and atmosphere of decarbonylation. Thus, the family of samples reported here provides a basis for determining how the catalytic activity depends on the cluster or aggregate size and the conditions of pretreatment of the γ-Al_2O_3 support.

Possible Causes of Aggregation of Supported Iridium

The data demonstrate that H_2 treatment led to rapid decarbonylation of the γ-Al_2O_3-supported $[Ir_4(CO)_{12}]$ accompanied by aggregation of the iridium (Fig. 4). To explain the more rapid aggregation of the supported clusters in H_2 relative to that in He, we note that H_2 reacts with carbonyl ligands as in Fischer–Tropsch synthesis (23), resulting in the formation of water (as well as volatile hydrocarbons), which affects the γ-Al_2O_3 surface composition and the rate of aggregation of the iridium. Water would be expected to have led to hydroxylation of the γ-Al_2O_3 surface, and there is evidence (24) that increasing surface hydroxylation facilitates migration of supported metals.

Recarbonylation of γ-Al_2O_3-Supported Iridium Clusters

The data reported in this paper, together with those published separately (10), clearly show that the choice of

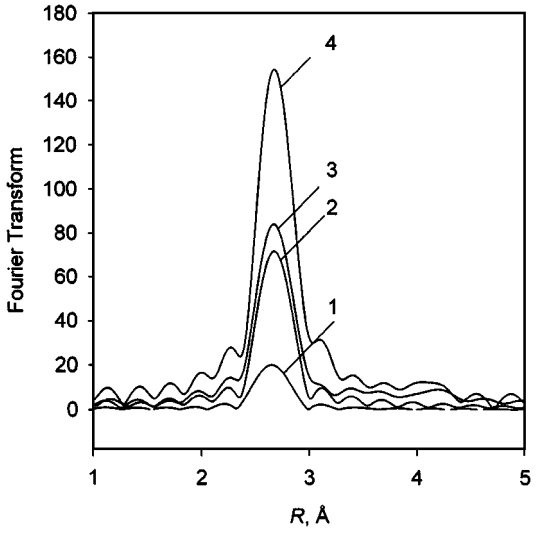

FIG. 4. Magnitude of the phase- and amplitude-corrected Fourier transform (k^3 weighted, $\Delta k = 3.61$–15.00 $Å^{-1}$) of the raw data illustrating increasing Ir–Ir first-shell coordination number of the surface species formed from $[Ir_4(CO)_{12}]/\gamma$-Al_2O_3 after treatment in H_2 under the following conditions: 1, 100°C; 2, 200°C; 3, 400°C; and 4, in O_2 at 300°C followed by H_2 at 400°C.

procedure used to remove carbonyl ligands from γ-Al_2O_3-supported $[Ir_4(CO)_{12}]$ substantially influences the structure of the resultant surface species, which, in turn affects the structure of the recarbonylated species. Infrared and EXAFS data characterizing γ-Al_2O_3-supported iridium clusters and aggregates show that partial reconstruction of the original γ-Al_2O_3-supported $[Ir_4(CO)_{12}]$ was possible only when the sample had been decarbonylated in He (at 300°C) to form surface species modeled (on the basis of EXAFS spectroscopy) as Ir_4 (10). If we assume that the reconstruction of the metal carbonyl clusters on γ-Al_2O_3 proceeds as it does in NaY zeolite (possibly through oxidative fragmentation leading to the formation of mononuclear iridium carbonyls, which then form $[Ir_4(CO)_{12}]$ (25)), then we might expect recarbonylation of iridium clusters with nuclearities larger than 4 also to give $[Ir_4(CO)_{12}]$. However, this was not observed, and the suggested analogy seems not to hold. We suggest that, under our conditions, the rates of oxidative fragmentation were negligible and that simple carbonylation of the supported clusters occurred at a much higher rate.

Thus, we might suggest that the nuclearity of the γ-Al_2O_3-supported and decarbonylated iridium species is important in affecting the decarbonylation/recarbonylation process. But we also recognize that the interactions of the iridium clusters and aggregates with the support probably influence the chemistry of the decarbonylation/recarbonylation process as well. XANES data reported for γ-Al_2O_3-supported iridium samples with different dispersions indicate an increase in the white line intensity with decreasing iridium cluster or aggregate size (21). These data are consistent with the postulate that metal–support interactions contribute to the electronic configuration of supported iridium, with the iridium clusters being more electron deficient than the larger aggregates (26, 27). Furthermore, the infrared and EXAFS data confirm the suggestion and show that the interactions of CO with iridium clusters (such as Ir_4) and with iridium aggregates containing tens of atoms are different as well. When CO was adsorbed at 25°C on the sample decarbonylated in He at 300°C and having an average Ir–Ir first-shell coordination number of 3.0 (and modeled as Ir_4), the υ_{CO} assigned to terminal CO species were observed at 2076 and 2002 cm^{-1} (10). In contrast, when the samples treated in H_2 and characterized by average Ir–Ir first-shell coordination numbers of 5.1 or larger were exposed to CO at 25–200°C, only a single terminal υ_{CO} band was observed, at 2058 cm^{-1} (Fig. 2). We infer that the appearance of two υ_{CO} bands in the infrared spectra after CO adsorption on clusters modeled as Ir_4 is a result of coordination of more than one CO molecule, on average, per Ir atom. Furthermore, the value of υ_{CO} observed for these Ir_4 clusters (2076 cm^{-1}) (10) is observed at a higher frequency than that (2058 cm^{-1}) observed for the larger iridium aggregates (Fig. 2), which indicates that the clusters are more electron deficient than the aggregates. We emphasize that only these highly dispersed iridium clusters, modeled as Ir_4 on the basis of EXAFS spectroscopy, were partially recarbonylated in CO at higher temperatures to give surface species with structures similar to that of $[Ir_4(CO)_{12}]$ (10).

Thus, in summary, the infrared and EXAFS data show that reversible decarbonylation/recarbonylation of $[Ir_4(CO)_{12}]$ supported on partially dehydroxylated γ-Al_2O_3 was possible, at least in part, but only when the nuclearity of the decarbonylated surface species matched that of the original iridium carbonyl cluster and the electronic configuration of the decarbonylated iridium species somehow facilitated adsorption of multiple CO ligands on iridium atoms to organize surface carbonyl species similar to those in the original $[Ir_4(CO)_{12}]$.

Catalytic Properties of Iridium Clusters and Aggregates for Toluene Hydrogenation

The least active catalyst in the family of supported iridium clusters and aggregates was that incorporating iridium clusters having an Ir–Ir first-shell coordination number of about 3 and approximated as Ir_4 (Table 3). The data are consistent with the inference that the turnover frequency depends on the cluster or aggregate size and not the decarbonylation conditions; the two samples with nearly the same average cluster size, one prepared by decarbonylation in He at 400°C and the other in H_2 at 200°C, have catalytic activities for toluene hydrogenation that are indistinguishable from each other within the expected experimental error (Table 3). (We expect that uncertainty in turnover frequencies could be as much as about 20–30%, estimated on the basis of errors in the EXAFS results and the reaction rates.)

The data clearly show a strong dependence of catalytic activity of iridium on the cluster or aggregate size, even though this is a structure-insensitive reaction (28, 29). A comparable set of data has been reported for a family of iridium clusters and aggregates on uncalcined γ-Al_2O_3 prepared by decarbonylation of $[Ir_4(CO)_{12}]$ at 300°C in He, followed by treatment in H_2 at 300–400°C for various times to give clusters and aggregates of various average sizes (9). Each set of data shows that the catalytic activity depends on the cluster or aggregate size. The results are qualitatively similar, showing an increase in activity of between one and two orders of magnitude as the average cluster or aggregate size increased from about 5.4 Å to more than about 30 Å.

However, the quantitative results for the two families of catalysts are different from each other. Table 4 provides a comparison of the catalytic data for the samples with (nearly) the same dispersion from each family of catalysts, one made from calcined γ-Al_2O_3 and the other from uncalcined γ-Al_2O_3. There is a difference of as much as an order of magnitude in activities at a given cluster or small

aggregate size, with the samples made from the calcined γ-Al_2O_3 being the more active. However, a comparison of the turnover frequencies characterizing the larger aggregates or particles of iridium in the two families indicates that the difference in activity was only a factor of several (Table 4).

Thus, the data raise two questions: Why does the catalytic activity depend on the cluster or aggregate size and why does it depend on the calcination temperature of the γ-Al_2O_3 support? Suggestions about the first question have already been published (9, 30). The issue is not resolved; perhaps the greater electron deficiency of the smallest clusters accounts in part for their lower catalytic activities.

In regard to the effect of the γ-Al_2O_3 calcination temperature, it is tempting to suggest that the water or hydroxyl group content of the uncalcined γ-Al_2O_3 may have influenced the catalytic activity—this might be a ligand effect. This supposed effect would be expected to be greater for the small iridium clusters than for the larger aggregates, consistent with the observations (Table 4). However, because catalytic data characterizing iridium clusters supported on MgO indicate a near lack of an effect of the surface hydroxyl content on the catalytic activity for toluene hydrogenation (16), we discount this interpretation.

Alternatively, we might speculate that when uncalcined γ-Al_2O_3 was used for sample preparation, some physical changes of the support (such as sintering with loss of surface area) might have occurred upon heating during the $[Ir_4(CO)_{12}]$ decarbonylation step. As a consequence, part of the iridium clusters might have bonded to the support (or even been incorporated within it) in such a way as to limit access of the reactants to the catalytic sites of the clusters and aggregates, with the effect being greatest for the smallest clusters and aggregates. This explanation is consistent with the data.

Chemisorption data characterizing the samples prepared on uncalcined γ-Al_2O_3 (9) show relatively low uptakes of hydrogen, always <1 H : Ir atom. These results might be interpreted to suggest that the surfaces of the clusters were partially occluded (consistent with the suggestion above) or that they were partially blocked by residues (perhaps carbon) remaining from the CO ligands of the precursor. As the treatments in H_2 would be expected to have led to less surface blockage by carbon or carbonaceous material than treatment in He (because hydrogenation occurred in the presence of H_2 but presumably not in the presence of He), one would expect the hydrogen chemisorption to be greater on the samples treated in H_2. However, because similarly low H : Ir ratios have been observed for the samples with nearly the same average cluster or aggregate size, independent of whether the treatment was in He or H_2 (31), we doubt that surface blockage by residues is a correct interpretation of the difference in catalytic activities between the two families of the samples.

In summary, the data indicate that clusters approximated as Ir_4 and larger iridium aggregates catalyze toluene hydrogenation, and the catalytic activity increases with cluster or aggregate size up to about 30 Å in average diameter. The activity of γ-Al_2O_3-supported iridium clusters and aggregates depends on the calcination temperature of the support, and it is not clear why. The data suggest that support calcination might be a useful tool in tuning properties of highly dispersed metal clusters.

ACKNOWLEDGMENTS

The research was supported in part by the National Science Foundation (Grant CTS-9615257). We acknowledge the Stanford Synchrotron Radiation Laboratory for access to beam time on beam line 2–3. We also acknowledge beam time and the support of the U.S. Department of Energy, Division of Materials Sciences, under Contract DE-FG05-89ER45384 for its role in the operation and development of beam line X-11A at the National Synchrotron Light Source. The NSLS is supported by the Department of Energy, Division of Materials Sciences and Division of Chemical Sciences, under Contract DE-AC02-76CH00016. We are grateful to the staff of beam line X-11A for their assistance. The EXAFS data were analyzed with the XDAP software developed by Vaarkamp *et al.* (12).

REFERENCES

1. Bernard, J. R., *in* "Proc. 5th Int. Zeolite Conf." (Rees, L. V. C., Ed.), p. 686. Heyden, London, 1986.
2. Hughes, T. R., Buss, W. C., Tamm, P. W., and Jacobson, R. L., *in* "New Developments in Zeolite Science and Technology" (Y. Murakami, A. Iijima, and J. W. Ward, Eds.), p. 725. Elsevier, Amsterdam, 1986.
3. Vaarkamp, M., Grondelle, J. V., Miller, J. T., Sajkowski, D., Modica, F. S., Lane, G. S., Gates, B. C., and Koningsberger, D. C., *Catal. Lett.* **6**, 369 (1990).
4. Vaarkamp, M., Modica, F. S., Miller, J. T., and Koningsberger, D. C., *J. Catal.* **144**, 611 (1993).
5. Miller, J. T., Meyers, B. L., Modica, F. S., Lane, G. S., Vaarkamp, M., and Koningsberger, D. C., *J. Catal.* **143**, 395 (1993).
6. *Oil Gas J.* **90**, 30 (1992).
7. Rotman, D., *Chem. Week* **8**, 150 (1992).
8. Gates, B. C., *Chem. Rev.* **95**, 511 (1995).
9. Xiao, F.-S., Weber, W. A., Alexeev, O., and Gates, B. C., *in* "Proceedings of the 11th International Congress on Catalysis" (J. W. Hightower, W. N. Delgass, E. Iglesia, and A. T. Bell, Eds.), Part B, p. 1135. Elsevier, Amsterdam, 1996.
10. Alexeev, O., Panjabi, G., and Gates, B. C., *J. Catal.* **173**, 196 (1998).
11. Jentoft, R. E., Deutsch, S. E., and Gates, B. C., *Rev. Sci. Instrum.* **67**, 2111 (1996).
12. Vaarkamp, M., Linders, J. C., and Koningsberger, D. C., *Physica B* **209**, 159 (1995).
13. Kirlin, P. S., van Zon, F. B. M., Koningsberger, D. C., and Gates, B. C., *J. Phys. Chem.* **94**, 8439 (1990).
14. van Zon, J. B. A. D., Koningsberger, D. C., van't Blik, H. F. J., and Sayers, D. E., *J. Chem. Phys.* **82**, 5742 (1985).
15. Koningsberger, D. C., and Prins, R. (Eds.), "X-Ray Absorption: Principles, Applications, Techniques of EXAFS, SEXAFS and XANES," Wiley, New York, 1988.
16. Deutsch, S. E., Mestl, G., Knözinger, H., and Gates, B. C., *J. Phys. Chem.* **101**, 1374 (1997).
17. Koningsberger, D. C., *in* "Synchrotron Techniques in Interfacial Electrochemistry" (C. A. Melendres and A., Tadjeddine Eds.), p. 181. Kluwer, Dordrecht, 1994.

18. Adams, D. M., and Taylor, I. D., *J. Chem. Soc., Faraday Trans. 2* **78**, 1573 (1982).
19. Tanaka, K., Watters, K. L., and Howe, R. F., *J. Catal.* **75**, 23 (1982).
20. Zhao, A., and Gates, B. C., *J. Am. Chem. Soc.* **118**, 2458 (1996).
21. Zhao, A., and Gates, B. C., *J. Catal.* **168**, 60 (1997).
22. Kip, B. J., Duivenvoorden, F. B. M., Koningsberger, D. C., and Prins, R., *J. Catal.* **105**, 26 (1987).
23. Smith, A. K., Theolier, A., Basset, J.-M., Ugo, R., Commereuc, D., and Chauvin, Y., *J. Am. Chem. Soc.* **100**, 2590 (1978).
24. Triantafillou, N. D., and Gates, B. C., *J. Phys. Chem.* **98**, 8431 (1994).
25. Beutel, T., Kawi, S., Purnell, S. K., Knözinger, H., and Gates, B. C., *J. Phys. Chem.* **97**, 7284 (1993).
26. Lytle, F. W., Wei, P. S. P., Greegor, R. B., Via, G. H., and Sinfelt, J. H., *J. Chem. Phys.* **70**, 4849 (1979).
27. Lytle, F. W., *J. Catal.* **43**, 376 (1976).
28. Boudart, M., and Djéga-Mariadassou, G., "Kinetics of Heterogeneous Catalytic Reactions," Princeton Univ. Press, Princeton, NJ, 1984.
29. Che, M., and Bennett, C. O., *Advan. Catal.* **36**, 55 (1989).
30. Xu, Z., Xiao, F.-S., Purnell, S. K., Alexeev, O., Kawi, S., Deutsch, S. E., and Gates, B. C., *Nature (London)* **372**, 346 (1994).
31. Alexeev, O., and Gates, B. C., to be published.